



A novel low Cr-containing Fe–Cr–Co alloy for metallic interconnects in planar intermediate temperature solid oxide fuel cells



Wenying Zhang ^{a, b}, Dong Yan ^{a, *}, Jie Yang ^{a, b}, Jing Chen ^{a, c}, Bo Chi ^a, Jian Pu ^a, Jian Li ^a

^a Center for Fuel Cell Innovation, School of Materials Science and Engineering, Huazhong University of Science & Technology, Wuhan 430074, China

^b Faculty of Mechanical and Electronic Information, China University of Geosciences, Wuhan 430074, China

^c School of Chemistry and Chemical Engineering, Henan University of Technology, Zhengzhou 450001, China

HIGHLIGHTS

- A novel low Cr-containing Fe–Cr–Co alloy is evaluated as a potential interconnect material.
- The alloy possesses excellent oxidation resistance and adequate electrical conductivity.
- The alloy exhibits slight Cr deposition in/around LSM electrode under accelerating condition.

ARTICLE INFO

Article history:

Received 3 April 2014

Received in revised form

24 July 2014

Accepted 25 July 2014

Available online 4 August 2014

Keywords:

Solid oxide fuel cells
Metallic interconnect
Oxidation resistance
Chromium deposition
Area specific resistance

ABSTRACT

A newly developed low-Cr containing Fe–Cr–Co alloy, named as FeCro, is evaluated as a candidate material of metallic interconnects for intermediate temperature solid oxide fuel cells (IT-SOFCs). This alloy possesses excellent oxidation resistance and adequate electrical conductivity at 750 °C in air, and shows slight Cr deposition in/around La_{0.72}Sr_{0.18}MnO₃(LSM) electrode under a harsh accelerating condition of 400 mA cm^{−2} and 850 °C. The thickness of the oxide scale thermally grown at 750 °C in air for 1000 h is less than 1 μm, presenting a double-layered structure with dense (Mn, Cr)₃O₄ on the top of Cr₂O₃. The oxidation kinetics at 750 °C obeys the parabolic law with a low rate constant of $1.42 \times 10^{-15} \text{ g}^2 \text{ cm}^{-4} \text{ s}^{-1}$. The Cr deposition in/around the LSM electrode in the presence of the FeCro alloy is remarkably reduced, compared to the commercial Crofer 22H alloy. The measured area specific resistance (ASR) at 750 °C in air after 1000 h isothermal oxidation is 14 mΩ cm². It is the unique microstructure of the formed oxide scale that significantly enhances the resistances of the FeCro alloy to oxidation and Cr volatilization.

© 2014 Elsevier B.V. All rights reserved.

1. Introduction

Interconnects are a key component in planar solid oxide fuel cell (SOFC) stacks, connecting neighboring cells electrically and separating the fuel from air physically. As SOFC operating temperature decreases to the intermediate temperature (IT) range between 600 and 800 °C, metallic alloys are considered as the candidate materials for the interconnects due to their high electrical and thermal conductivities, robust mechanical properties, easy fabricability and low cost [1–3].

The most widely used metallic alloys are Cr₂O₃-forming ferritic stainless steels, such as AISI 430 (~16 wt. % Cr) and Crofer 22H

(~22 wt. % Cr), which have a coefficient of thermal expansion (CTE) closely matched to the cell components, and forms a conductive double-layered oxide scale upon operation with a layer of loosely packed (Mn, Cr)₃O₄ on the top of dense Cr₂O₃ [4–8]. However, they are still lack of sufficient oxidation resistance and conductivity, and possibly causes cathode poisoning by Cr evaporated from the oxide scale; improvements by surface modifications or coatings are often required for a long-term application [9–16] with added fabrication complexity and extra cost. Thus the development of new alloys [5,8,17–22] is extremely desired.

In the present study, a newly developed Fe–Cr–Co alloy (named as FeCro) was evaluated as a material for the metallic interconnects of IT-SOFCs. It contains Fe (balance), 12.44 wt. % of Cr, 9.68 wt. % of Co and small amounts of Mn, Zr, La and Y (Table 1). The decrease in the Cr amount of this alloy was to improve the conductivity and reduce Cr volatilization of the formed oxide scale; and the addition

* Corresponding author. Tel.: +86 27 87557694; fax: +86 27 87558142.

E-mail address: yand@hust.edu.cn (D. Yan).

Table 1
Chemical compositions of FeCro and Crofer 22H alloys (wt. %).

	Cr	Co	Mo	Mn	Zr	La	Y	C	S	P	Si	N	W	Nb	Ti	Cu
FeCro	12.44	9.68		0.57	0.024	0.0074	0.0014	0.0031	0.0016	0.0088	0.032					
Crofer 22H	20–24			0.3–0.8		0.04–0.20		<0.03	<0.006	<0.05	0.1–0.6	<0.03	1.0–3.0	0.2–1.0	0.02–0.20	<0.5

of Co was to enhance oxidation resistance by increasing the activity and diffusivity of Cr element [23]. Reactive elements Zr, Y and La were expected to further increase the oxidation resistance and improve the adhesion between the oxide scale and the metallic substrate [24,25]. For comparison, commercially available metallic interconnect alloy Crofer22H (Table 1) was also evaluated under the same conditions.

2. Experimental

The FeCro alloy was prepared from pure constituent elements by using a vacuum induction furnace. The ingot was forged above 950 °C into 20 mm thick plate, which was then hot-rolled between 1150 and 950 °C to 3 mm and cold rolled to 1 mm, followed by annealing in vacuum at 800 °C for 1 h.

Oxidation specimens of the FeCro and Crofer 22H in a dimension of $1 \times 25 \times 25$ mm were prepared by cutting with a slow diamond saw and polishing with SiC papers up to 1200-grit, and then cyclically oxidized in ambient air at 750 °C for 1000 h. The heating and cooling rates were 5°C min^{-1} ; and 14 cycles were performed during test. The weight gain of specimen (ΔW) after each cycle was measured by an electronic balance. The phases formed in the oxide scale were identified by X-ray diffraction (X'Pert PRO) with $\text{CuK}\alpha$ radiation. A scanning electron microscope (SEM, Quanta 200) with an energy dispersive spectrometer (EDS) was used for analyzing the composition and examining the microstructure of the formed oxide scale. The coefficient of thermal expansion (CTE) of the FeCro was determined by a dilatometer (DIL-402C).

The area specific resistance (ASR) of the specimens isothermally oxidized at 750 °C in air for 1000 h was measured in air at temperatures from 500 to 850 °C by the four-point technique. Similar to what reported previously [19,26,27], Pt paste and mesh were used for collecting current, and Pt wire was used as the testing lead. A constant current at 200 mA cm^{-2} was applied by a power source (ITECH, IT6270), while the voltage drop across the oxidized specimen was measured by a voltage meter (LEEF, ZYB-1). The value of ASR was calculated by the Ohm's Law.

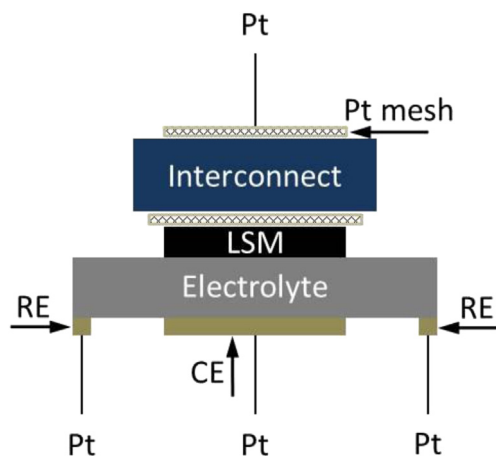


Fig. 1. Schematic testing setup for Cr deposition test.

In order to evaluate the Cr volatilization from the formed oxide scale and deposition into the cathode, a specimen setup similar to what reported by Wu et al. [28] was employed, as shown in Fig. 1. The electrolyte pellet was prepared with 8 mol.% Y_2O_3 stabilized ZrO_2 powder (YSZ, Tosoh) by die pressing and subsequent sintering at 1500 °C in air for 3 h. The $\text{La}_{0.72}\text{Sr}_{0.18}\text{MnO}_3$ (LSM) electrode was prepared by screen printing LSM slurry (formulated in-house) on the YSZ pellet, followed by sintering at 1100 °C in air for 2 h. The thickness of the electrode was approximately 7 μm and the active area was 0.5 cm^2 . Pt paste, as counter and reference electrodes, was painted on the other side of the YSZ pellet opposite to the electrode. A piece of FeCro or Crofer 22H in a dimension of $10 \times 10 \times 1$ mm was compressively placed on top of the electrode with Pt mesh in between. During the Cr volatilization/deposition test at 850 °C, electrical current at 400 mA cm^{-2} was applied for 24 h. The surface microstructure and composition of the LSM electrode and underneath YSZ substrate were examined by a field emission scanning electron microscope (FESEM, Sirion 200) and/or a secondary ion mass spectrometer (ION-TOF GmbH, Münster, Germany).

3. Results and discussion

Fig. 2 shows the thermal expansion curve of the FeCro at temperatures between 25 and 1000 °C, demonstrating a phase transformation from body-centered-cubic ferrite to face-centered-cubic austenite between 734 and 753 °C. The average CTE of the ferrite phase between 25 and 734 °C is $11.9 \times 10^{-6} \text{ K}^{-1}$, which is well matched to that of the cell components; the average CTE of the austenite phase at temperatures above 753 °C is $22.1 \times 10^{-6} \text{ K}^{-1}$, which is significantly higher than that of the cell components. However, for a planar SOFC stack operated at 900 °C, the maximum dimension change of the interconnect caused by the transformation is only 0.32% (indicated by dashed lines in Fig. 2), which most probably will not lead to the breakage of the cell that is in

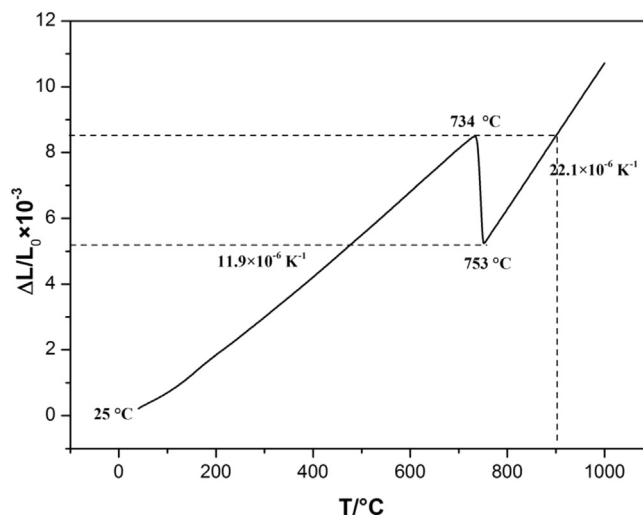


Fig. 2. Thermal expansion behavior of the FeCro alloy.

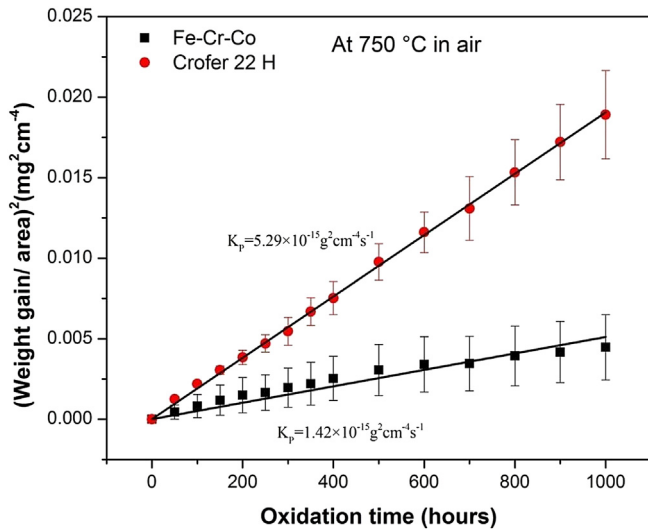


Fig. 3. Oxidation weight gain of FeCrCo and Crofer 22H alloys as a function of oxidation time at 750 °C in air.

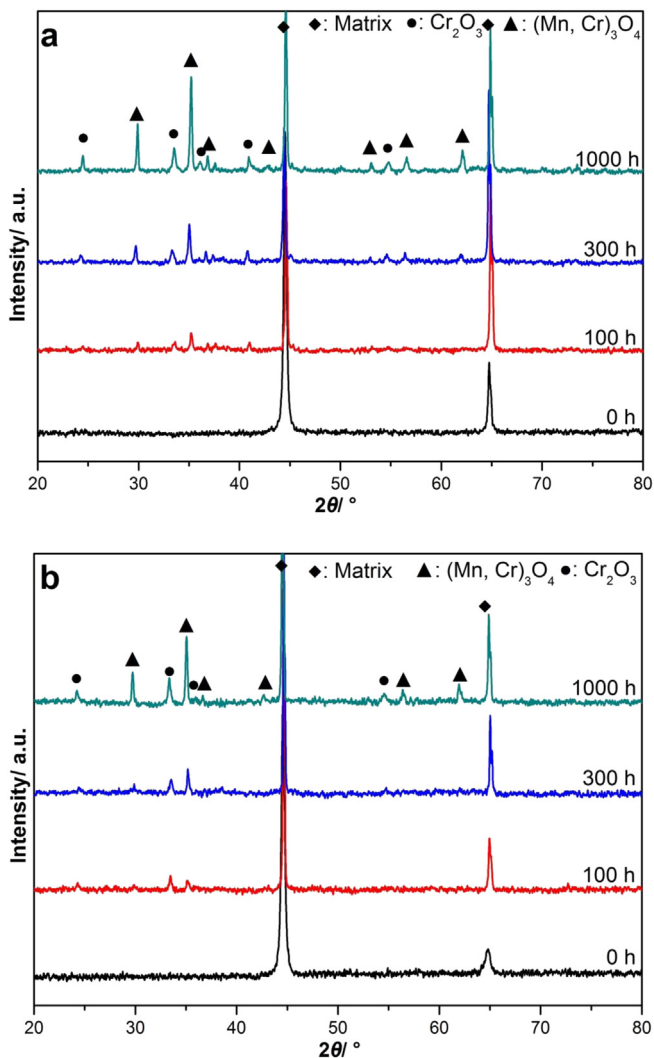


Fig. 4. XRD patterns of Crofer 22H (a) and FeCrCo (b) alloys oxidized at 750 °C in air for different periods of time.

contact with the interconnect under compressive load through a layer of powdery contact material. Whether the CTE difference between the FeCro interconnect and cell leads to cell breakage will be a topic of further study.

3.1. Oxidation resistance

During the cyclic oxidation at 750 °C in air for up to 1000 h, the weight gain ΔW of the specimens increased with time (t), as shown in Fig. 3 for the FeCro and Crofer 22H alloys. The error bar was generated by using the data obtained from 3 different specimens. The oxidation kinetics of both the alloys followed the parabolic law.

$$\left(\frac{\Delta W}{A}\right)^2 = K_p t \quad (1)$$

where A is the surface area of the specimen and K_p is the rate constant. The obtained value of average K_p for the FeCro alloy was

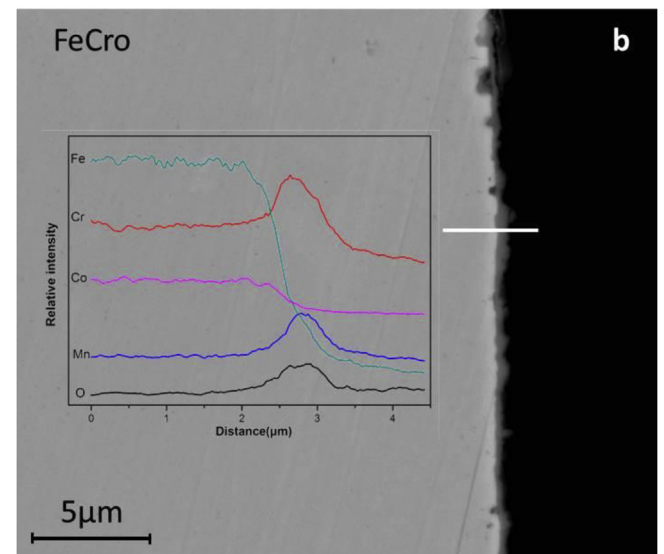
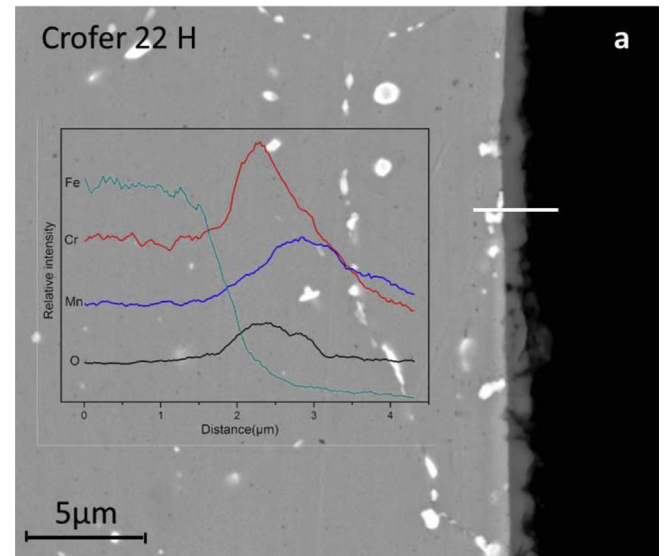


Fig. 5. SEM back-scattering images and line-scan analysis of cross-sectioned Crofer 22H (a) and FeCrCo (b) alloys oxidized at 750 °C for 1000 h in air.

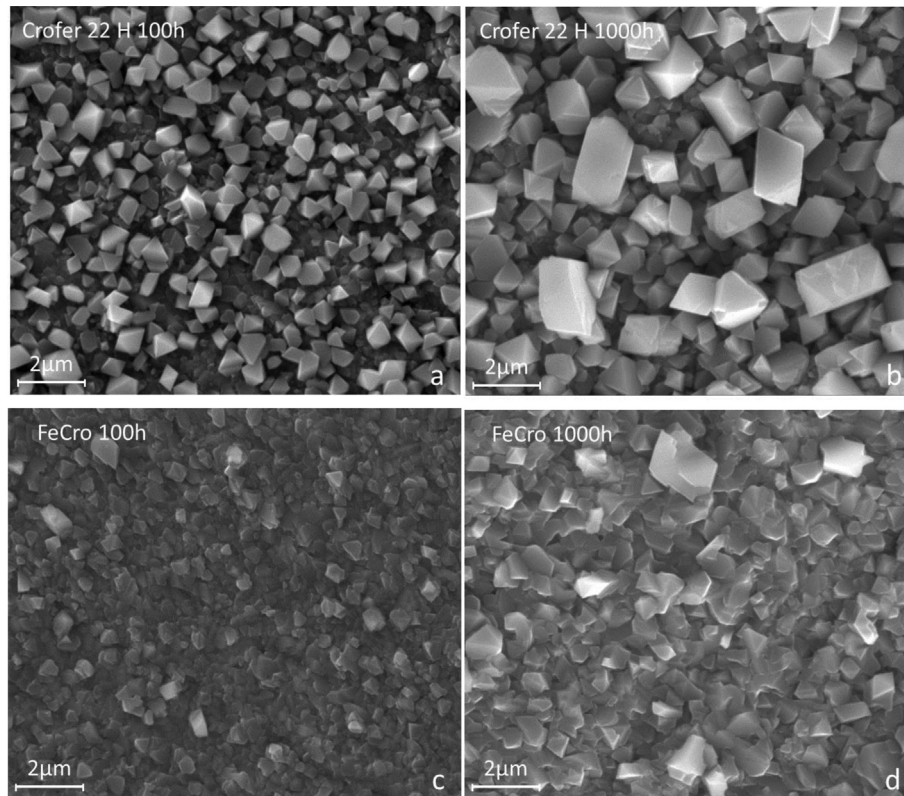


Fig. 6. Surface oxide morphologies of Crofer 22H and FeCro alloys oxidized at 750 °C in air for 100 h (a, c) and 1000 h (b, d), respectively.

$1.42 \times 10^{-15} \text{ g}^2 \text{ cm}^{-4} \text{ s}^{-1}$, which was only 1/4 of that for Crofer 22H ($5.29 \times 10^{-15} \text{ g}^2 \text{ cm}^{-4} \text{ s}^{-1}$) and one to two orders of magnitude lower than that for AISI 430 [6]. This result confirms that the oxidation resistance of the FeCro alloy at 750 °C in air is significantly higher than that of the conventional interconnect alloys.

The XRD patterns generated from the FeCro and Crofer 22H alloys oxidized at 750 °C in air for up to 1000 h are shown in Fig. 4, which indicates that the oxide scale formed on the surfaces of both the alloys were consisted of $(\text{Mn, Cr})_3\text{O}_4$ and Cr_2O_3 phases, and the thickness of the oxide scale, reflected by the intensity of diffraction peaks, increased with oxidation time. It is also seen that the peak intensity diffracted from the surface of the oxidized Crofer 22H (Fig. 4a) was stronger than that of the oxidized FeCro (Fig. 4b), implying that a thicker oxide scale was formed on the surface of Crofer 22H, as suggested by the result of oxidation kinetics.

Fig. 5 shows the cross-sectional microstructure and compositional profile of the FeCro and Crofer 22H oxidized at 750 °C in air for 1000 h. It is indeed true that the oxide scale formed on the surface of Crofer 22H ($\sim 2 \mu\text{m}$, Fig. 5a) was much thicker, more than twice as that of the FeCro ($< 1 \mu\text{m}$, Fig. 5b). The composition of the oxide scale was similar for these two alloys, containing Mn, Cr and O elements distributed in the inner layer of Cr_2O_3 and the outer layer of $(\text{Mn, Cr})_3\text{O}_4$. However, the surface morphology of the oxide scale was obviously different, as shown in Fig. 6. The cubic-structured $(\text{Mn, Cr})_3\text{O}_4$ particles on the surface of oxidized Crofer 22H was loosely packed and grew fast during the 1000 h test with some much larger particles decorated on the top (Figs. 6a and b). In contrast, the oxide particles on the surface of oxidized FeCro were densely packed and grew moderately and uniformly (Fig. 6c and d). It is expected that the formation of the dense oxide scale on the FeCro alloy is a result of increased Cr activity and diffusivity in the alloy, and the dense oxide scale slowed down the inward transport of O_2 in air, significantly enhancing the oxidation resistance for the FeCro alloy.

3.2. Electrical conductivity of the oxide scale

Fig. 7 is the Arrhenius plot of the area specific resistance (ASR) contributed by the oxide scale formed on the FeCro alloy after 1000 h isothermal oxidation. The data were obtained by using the oxidized specimen with the weight gain close to the average shown in Fig. 3. $\log(\text{ASR}/T)$ was linearly proportional to T^{-1} , showing the electrical behavior of semi-conductors. The value of ASR was from 10.6 to 68.4 $\text{m}\Omega \text{ cm}^2$ in the temperature range from 500 to 850 °C. At 800 °C, it was 11.8 $\text{m}\Omega \text{ cm}^2$, which is lower than

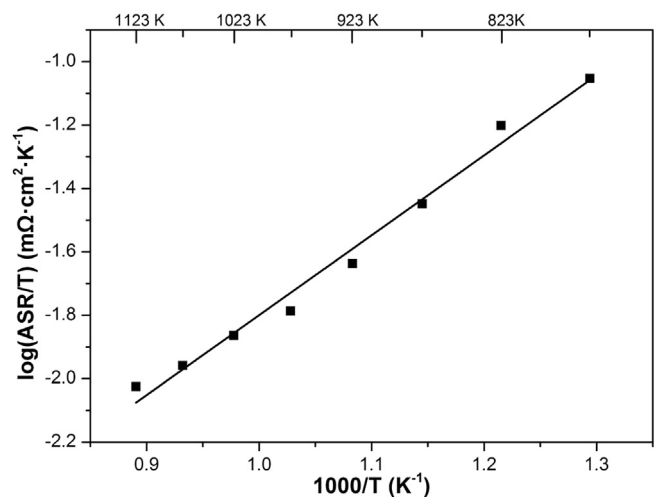


Fig. 7. Area specific resistance of FeCro alloy as a function of measurement temperature. The specimen was pre-oxidized at 750 °C in air for 1000 h.

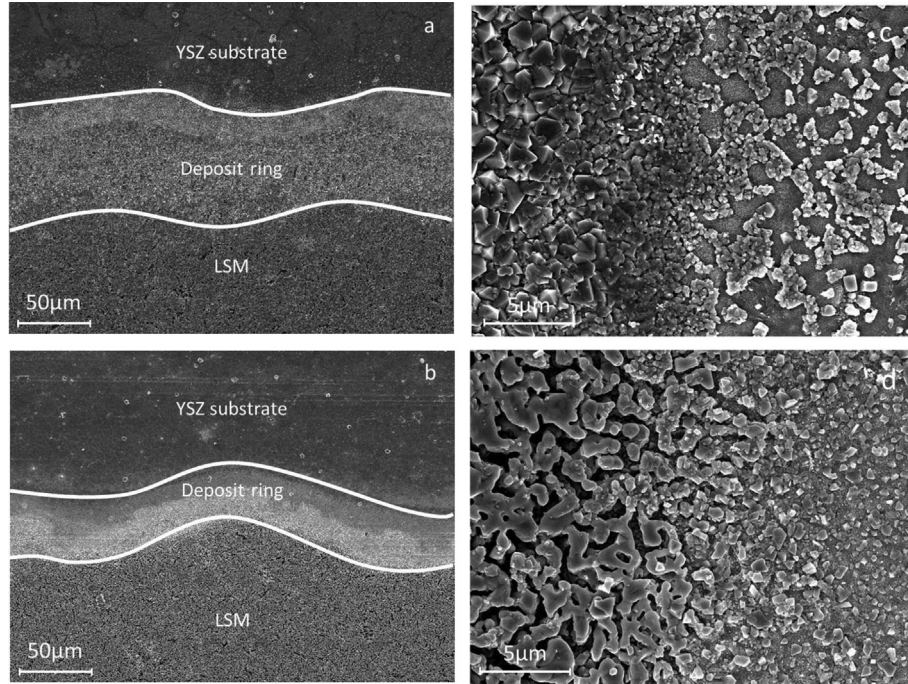


Fig. 8. SEM micrographs showing the deposits formed in the area near the edge of LSM electrode in the presence of Crofer 22H (a, c) and FeCro (b, d) alloys at 400 mA cm^{-2} and 850°C for 24 h.

that of Crofer 22H oxidized in air for only 300 h ($17.1 \text{ m}\Omega \text{ cm}^2$) [29].

Usually the thickness of formed oxide scale (Δl) is proportional to weight gain (ΔW) of the specimen, i.e.

$$\Delta l \propto \Delta W \quad (2)$$

From the expression of oxidation kinetics, Eq. (1), ΔW^2 is proportional to the product of the rate constant k_p and oxidation time t ; therefore,

$$\Delta l \propto (k_p t)^{1/2} \quad (3)$$

By definition,

$$\text{ASR} = \rho \Delta l \quad (4)$$

where ρ is the resistivity of the oxide scale. As a result,

$$\text{ASR} \propto \rho (k_p t)^{1/2} \quad (5)$$

Assuming the rate constant k_p and the resistivity ρ remain unchanged in prolonged oxidation, it can be reasonably obtained that,

$$\text{ASR} \propto t^{1/2} \quad (6)$$

According to Eq. (6), the ASR of the oxide scale formed on the FeCro alloy after oxidation at 750°C in air for 40,000 h (conventional life design for SOFCs) will be $88.5 \text{ m}\Omega \text{ cm}^2$, which is lower than $100 \text{ m}\Omega \text{ cm}^2$, the maximum limit requirement for metallic interconnects [3]. This result indicates that the FeCro alloy is a promising material for metallic interconnects used for IT-SOFCs in terms of the resistance to oxidation and ASR of the formed oxide scale.

3.3. Chromium deposition

Other than oxidation resistance and conductivity of formed oxide scale, cathode-poisoning, caused by Cr volatilization from the oxide scale formed on the surface of metallic interconnects and subsequent deposition in the cathode, is another major concern in material selection for the interconnect applications. Therefore, the Cr deposition in LSM electrode was evaluated comparatively for both the FeCro and Crofer 22H alloys at 850°C in ambient air. Fig. 8 shows the SEM microstructure of the deposits formed on the YSZ substrate in the surrounding area near the edge of LSM electrode (deposit ring) after current passage at 400 mA cm^{-2} and 850°C for 24 h. With the Crofer 22H alloy in place, the width of the light-colored deposit ring formed on the YSZ substrate was averagely about $80 \mu\text{m}$ (Fig. 8a), which was more than twice the size of the ring formed in the presence of the FeCro alloy (Fig. 8b). Close examination revealed that the LSM electrode in contact with the Crofer 22H alloy was fully covered by prism-shaped $(\text{Mn, Cr})_3\text{O}_4$ (Fig. 8c), which was formed by the reaction between the deposited Cr and Mn in LSM, and the YSZ substrate within the ring was partially covered by Cr_2O_3 particles. Differently the top surface of the LSM electrode underneath the FeCro alloy was almost clean (Fig. 8d).

The interface between the LSM electrode and YSZ substrate was also examined after selectively removal of the LSM electrode by aqua regia. It is shown by Fig. 9a that the YSZ surface in contact with the LSM electrode was completely covered by a layer of small particles of $(\text{Mn, Cr})_3\text{O}_4$ and Cr_2O_3 after 24 h current passage at 400 mA cm^{-2} and 850°C in air in the presence of Crofer 22H. This observation suggests that the deposited oxide not only occupied the triple phase boundary, but also formed in between the electrolyte and electrode. As a consequence, the cell structure was changed and the cell performance would be deteriorated. With the FeCro alloy, the interface was remained with the imprint of the removed LSM electrode and sporadically distributed with fine particles, the composition of which was not able to be identified by EDS, as shown in Fig. 9b. By using SIMS, the information from Cr and

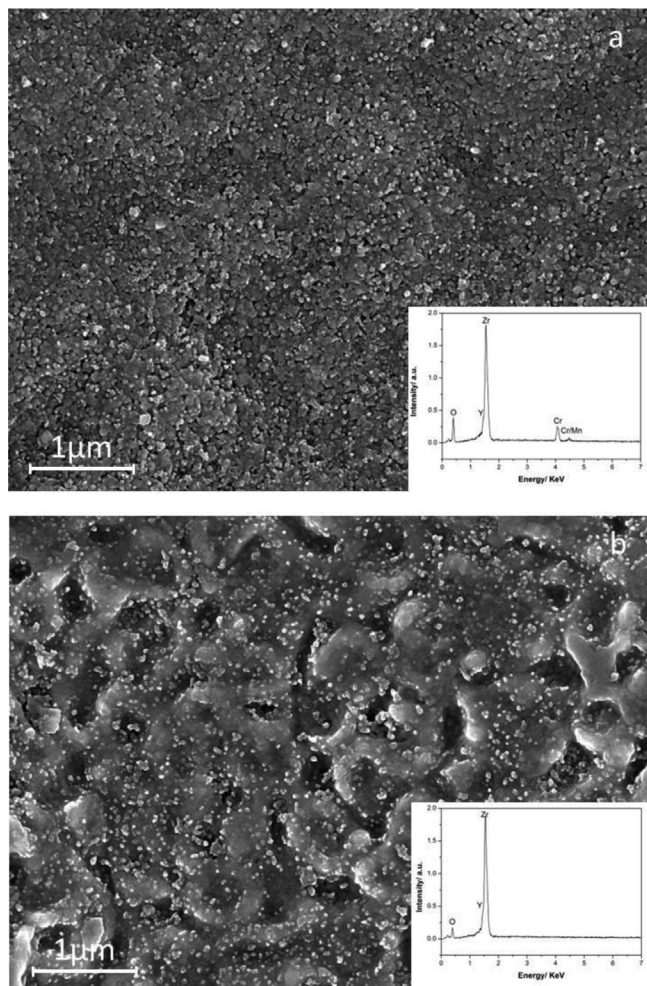


Fig. 9. Surface morphology of YSZ electrolyte in contact with LSM electrode. The electrode was polarized at 400 mA cm^{-2} and 850°C for 24 h in the presence of Crofer 22H (a) and FeCro (b) alloys and was dissolved by aqua regia. The inserts show the result of EDS analysis.

Mn was obtained from the interface, as shown in Fig. 10. According to the intensity change of each element with the sputtering time, it may be expected that the fine particles were $(\text{Mn}, \text{Cr})_3\text{O}_4$ formed on the YSZ substrate due to Cr deposition.

All the above results indicate that Cr deposition was significantly mitigated with the FeCro alloy. This can be explained by the difference in the microstructure of oxide scale formed alloy surface and the volatility of Cr in Cr_2O_3 and $(\text{Mn}, \text{Cr})_3\text{O}_4$. It is known that the Cr in $(\text{Mn}, \text{Cr})_3\text{O}_4$ is less volatile than that in Cr_2O_3 [30,31]; the thermally grown double-layer oxide scale with $(\text{Mn}, \text{Cr})_3\text{O}_4$ on the top of Cr_2O_3 is beneficial to depressing Cr volatilization from the oxide scale. The loosely packed outer $(\text{Mn}, \text{Cr})_3\text{O}_4$ layer, which is the case for the Crofer 22H alloy, cannot effectively prevent Cr volatilization from the inner Cr_2O_3 ; only a dense layer of $(\text{Mn}, \text{Cr})_3\text{O}_4$ as that formed on the surface of the FeCro alloy can serve the purpose.

4. Conclusions

A newly low-Cr containing alloy, the FeCro, was developed as a candidate interconnect material for IT-SOFCs; and the oxidation resistance at 750°C in air, conductivity of thermally grown oxide scale and Cr deposition in/around LSM electrode were evaluated, in comparison with the Crofer 22H alloy. Based on the obtained results, the following conclusions are made.

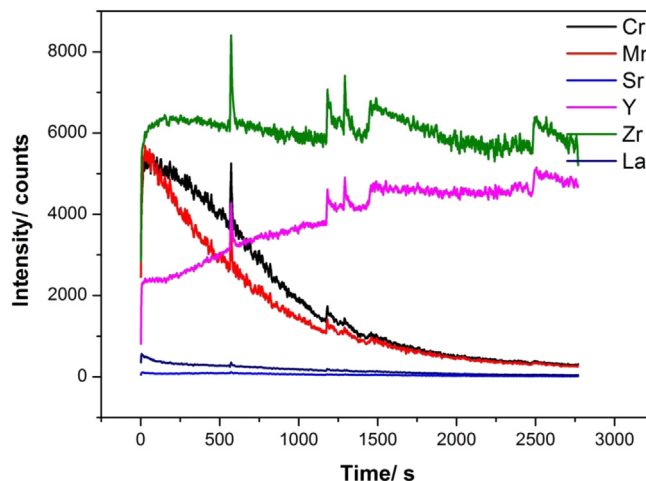


Fig. 10. SIMS analysis of the YSZ surface shown in Fig. 9.

- 1) The FeCro alloy has an average CET of $10.96 \times 10^{-6} \text{ K}^{-1}$ in the temperature range between 25 and 1000°C , which is well-matched to that of the cell components and appropriate for the application of interconnects in IT-SOFC.
- 2) The kinetics of cyclic oxidation of the FeCro alloy at 750°C in air obeys the parabolic law with a much smaller rate constant k_p than that of the conventional alloys for metallic interconnects. It forms a double-layer oxide scale with dense $(\text{Mn}, \text{Cr})_3\text{O}_4$ spinel on the top of Cr_2O_3 .
- 3) It is the dense outer $(\text{Mn}, \text{Cr})_3\text{O}_4$ that significantly enhances the resistances of the FeCro alloy to oxidation at 750°C in air and prevents Cr volatilization from the thermally grown oxide scale and deposition in/around the LSM electrode.
- 4) The ASR contributed by the oxide scale formed on the FeCro alloy follows the Arrhenius equation. The extrapolated value of ASR for oxidizing at 750°C in air for 40,000 h is $88.5 \text{ m}\Omega \text{ cm}^2$, which meets the requirement of $100 \text{ m}\Omega \text{ cm}^2$ for the life design of SOFCs.

Acknowledgments

This research was financially supported by the National Natural Science Foundation of China (51271083), the National “863” program (2011AA050702) and the National Natural Science Foundation of China (51102079). The SEM and XRD were performed with the assistance provided by the Analytical and Testing Center of Huazhong University of Science and Technology.

References

- [1] H. Yokokawa, N. Sakai, T. Horita, K. Yamaji, *Fuel Cells* 1 (2001) 117–131.
- [2] W.Z. Zhu, S.C. Deevi, *Mater. Sci. Eng. A* 348 (2003) 227–243.
- [3] J.W. Fergus, *Mater. Sci. Eng. A* 397 (2005) 271–283.
- [4] J. Rufner, P. Gannon, P. White, M. Deibert, S. Teintze, R. Smith, H. Chen, *Int. J. Hydrogen Energy* 33 (2007) 1392–1398.
- [5] B. Hua, J. Pu, F.S. Lu, J.F. Zhang, B. Chi, J. Li, *J. Power Sources* 195 (2010) 2782–2788.
- [6] J. Pu, J. Li, B. Hua, G.Y. Xie, *J. Power Sources* 158 (2006) 354–360.
- [7] S.J. Geng, J.H. Zhu, *J. Power Sources* 160 (2006) 1009–1016.
- [8] J. Froitzheim, G.H. Meier, L. Niewolak, P.J. Ennis, H. Hattendorf, L. Singheiser, W.J. Quadakkers, *J. Power Sources* 178 (2008) 163–173.
- [9] B. Hua, J. Pu, W. Gong, J.F. Zhang, F.S. Lu, J. Li, *J. Power Sources* 185 (2008) 419–422.
- [10] B. Hua, W.Y. Zhang, J. Wu, J. Pu, B. Chi, J. Li, *J. Power Sources* 195 (2010) 7375–7379.
- [11] W.Y. Zhang, J. Pu, B. Chi, J. Li, *J. Power Sources* 196 (2011) 5591–5594.
- [12] W.Y. Zhang, B. Hua, N.Q. Duan, J. Pu, B. Chi, J. Li, *J. Electrochem. Soc.* 159 (2012) C388–C392.

- [13] S. Fontana, S. Chevalier, G. Caboche, *Oxid. Met.* 78 (2012) 307–328.
- [14] L.C. Ajitdoss, F. Smeacetto, M. Bindi, D. Beretta, M. Salvo, M. Ferraris, *Mater. Lett.* 95 (2013) 82–85.
- [15] S.J. Geng, S.J. Qi, Q.C. Zhao, S.L. Zhu, F.H. Wang, *Int. J. Hydrogen Energy* 37 (2012) 10850–10856.
- [16] P. Yang, C.K. Liu, J.Y. Wu, W.J. Shong, R.Y. Lee, C.C. Sung, *J. Power Sources* 213 (2012) 63–68.
- [17] B. Hua, F.S. Lu, J.F. Zhang, Y.H. Kong, J. Pu, B. Chi, J. Li, *J. Electrochem. Soc.* 156 (2009) B1261–B1266.
- [18] P.D. Jablonski, D.E. Alman, *J. Power Sources* 180 (2008) 433–439.
- [19] B. Hua, J. Pu, F.S. Lu, J.F. Zhang, B. Chi, J. Li, *J. Electrochem. Soc.* 156 (2009) B93–B98.
- [20] S.J. Geng, J.H. Zhu, M.P. Brady, H.U. Anderson, X.D. Zhou, *J. Power Sources* 172 (2007) 775–781.
- [21] J.H. Zhu, S.J. Geng, D.A. Ballard, *J. Power Sources* 32 (2007) 3682–3688.
- [22] I. Antepara, I. Villarreal, L.M. Rodriguez-Martinez, N. Lecanda, U. Castro, A. Laresgoiti, *J. Power Sources* 151 (2005) 103–107.
- [23] J. Zurek, E. Wessel, L. Niewolak, F. Schmitz, T.U. Kern, L. Singheiser, W.J. Quadackers, *Corros. Sci.* 46 (2004) 2301–2317.
- [24] S.C. Tsai, A.M. Huntz, C. Dolin, *Mater. Sci. Eng. A* 212 (1996) 6–13.
- [25] C.M. Cotell, G.J. Yurek, R.J. Hussey, D.F. Mitchell, M.J. Graham, *Oxid. Met.* 34 (1990) 173–200.
- [26] Y. Liu, D.Y. Chen, *Int. J. Hydrogen Energy* 34 (2009) 9220–9226.
- [27] B. Hua, Y.H. Kong, F.S. Lu, J.F. Zhang, J. Pu, J. Li, *Chin. Sci. Bull.* 55 (2010) 3831–3837.
- [28] J. Wu, D. Yan, J. Pu, B. Chi, J. Li, *J. Power Sources* 202 (2010) 166–174.
- [29] L. Paul, H. Hattendorf, L. Niewolak, B. Kuhn, O. Ibas, W.J. Quadackers, in: *Fuel Cell Symposium*, San Antonio, TX, USA, 2010.
- [30] Z.G. Lu, J.H. Zhu, *J. Am. Ceram. Soc.* 88 (2005) 1050–1053.
- [31] S.P. Jiang, Y.D. Zhen, S. Zhang, A.L.Y. Tok, P. Wu, *J. Electrochem. Soc.* 153 (2006) A2120–A2125.